molecules

MDPI

*Article*

# Fast Li-Ion Conduction in Spinel-Structured Solids

**Jan L. Allen [1,*], Bria A. Crear [2], Rishav Choudhury [3], Michael J. Wang [3], Dat T. Tran [1], Lin Ma [1], Philip M. Piccoli [4], Jeff Sakamoto [3] and Jeff Wolfenstine [5]**

1 Energy Sciences Division, Sensors & Electron Devices Directorate, US Army Research Laboratory, Adelphi, MD 20783, USA; dat.t.tran4.civ@mail.mil (D.T.T.); liam.l.ma.civ@outlook.com (L.M.)
2 Department of Chemistry, Howard University, Washington, DC 20059, USA; bria.a.crear@gmail.com
3 Department of Materials Science and Engineering, University of Michigan, Ann Arbor, MI 48109, USA; rishavc@umich.edu (R.C.); micwan@umich.edu (M.J.W.); jeffsaka@umich.edu (J.S.)
4 Department of Geology, University of Maryland, College Park, MD 20742, USA; piccoli@umd.edu
5 Solid Ionic Consulting, 9223 Matthews Ave, Seattle, WA 98115, USA; jeffyspeak@outlook.com
* Correspondence: jan.l.allen8.civ@mail.mil

**Abstract:** Spinel-structured solids were studied to understand if fast $Li^+$ ion conduction can be achieved with Li occupying multiple crystallographic sites of the structure to form a "Li-stuffed" spinel, and if the concept is applicable to prepare a high mixed electronic-ionic conductive, electrochemically active solid solution of the $Li^+$ stuffed spinel with spinel-structured Li-ion battery electrodes. This could enable a single-phase fully solid electrode eliminating multi-phase interface incompatibility and impedance commonly observed in multi-phase solid electrolyte–cathode composites. Materials of composition $Li_{1.25}M(III)_{0.25}TiO_4$, M(III) = Cr or Al were prepared through solid-state methods. The room-temperature bulk $Li^+$-ion conductivity is $1.63 \times 10^{-4}$ S cm$^{-1}$ for the composition $Li_{1.25}Cr_{0.25}Ti_{1.5}O_4$. Addition of $Li_3BO_3$ (LBO) increases ionic and electronic conductivity reaching a bulk $Li^+$ ion conductivity averaging $6.8 \times 10^{-4}$ S cm$^{-1}$, a total Li-ion conductivity averaging $4.2 \times 10^{-4}$ S cm$^{-1}$, and electronic conductivity averaging $3.8 \times 10^{-4}$ S cm$^{-1}$ for the composition $Li_{1.25}Cr_{0.25}Ti_{1.5}O_4$ with 1 wt. % LBO. An electrochemically active solid solution of $Li_{1.25}Cr_{0.25}Mn_{1.5}O_4$ and $LiNi_{0.5}Mn_{1.5}O_4$ was prepared. This work proves that Li-stuffed spinels can achieve fast Li-ion conduction and that the concept is potentially useful to enable a single-phase fully solid electrode without interphase impedance.

**Keywords:** solid electrolyte; fast $Li^+$ ion conductor; Li-ion battery; spinel; solid-state battery; cathode-electrolyte interface



**Citation:** Allen, J.L.; Crear, B.A.; Choudhury, R.; Wang, M.J.; Tran, D.T.; Ma, L.; Piccoli, P.M.; Sakamoto, J.; Wolfenstine, J. Fast Li-Ion Conduction in Spinel-Structured Solids. *Molecules* **2021**, *26*, 2625. https://doi.org/10.3390/molecules26092625

Academic Editors: Stephane Jobic, Claude Delmas and Myung-Hwan Whangbo

Received: 18 March 2021
Accepted: 29 April 2021
Published: 30 April 2021



## 1. Introduction

Interest in solid-state electrolytes has intensified owing to the discovery of fast Li-ion conduction in the cubic garnet structure [1], the continued push for higher energy density batteries and the allure of the safety of an inorganic all solid-state battery. The spinel is a suitable cubic structure to search for fast Li-ion conduction owing to its network of empty edge-shared $MO_6$ octahedra bridged by face-shared $LiO_4$ tetrahedra, which connect in three dimensions thereby providing a path for 3D $Li^+$-ion conduction [2]. In fact, $LiMn_2O_4$ spinel's favorable mixed electronic-ionic conductivity has enabled its use as a positive electrode [2]. $LiMn_2O_4$ ideally crystallizes in the normal spinel structure in the $Fd\bar{3}m$ space group: Mn occupies the 16d octahedral site, O occupies the 32e position and Li occupies the 8a tetrahedral site which share faces with an empty 16c octahedral site within the spinel's pseudo-cubic closed packed oxygen framework, thus forming a three-dimensional 8a → 16c → 8a Li ion conduction pathway. Furthermore, the spinel's cubic unit cell is desirable for solid-state battery application since differences in thermal expansion coefficients of different crystallographic directions in large-grained non-cubic ceramic materials, may lead to micro-cracking [3–5] during cooling after densification which is unfavorable for mechanical properties and ionic conductivity [6–9]. Additionally,

the use of a spinel-structured solid electrolyte as a separator in an all solid-state battery and pursuit of high conductivity in the spinel structure can lead to insights that may improve rate capability of spinel structured electrodes for use with liquid based electrolytes or as a catholyte or anolyte in a fully solid-state configuration.

Limited work has been done on oxide spinel structured solid electrolytes. Kawai et al. discovered a conductivity of about $10^{-7}$ S cm$^{-1}$ for the ordered ($P_432$ space group) spinel $LiNi_{0.5}Ge_{1.5}O_4$ at 63 °C [10]. The Ni and Ge are ordered on the octahedral sites of this compound. In 1985, Thackeray and Goodenough proposed the all-solid all-spinel battery as a means to reduce interfacial impedance at the interface of the solid-state cathode, electrolyte and anode but did not identify a suitable solid-state electrolyte [11]. Rosciano et al. suggested the Li doped $MgAl_2O_4$ spinel as a potential solid-state electrolyte based on high Li diffusivity as measured by nuclear magnetic resonance (NMR) as a means to enable a full spinel concept [12]. However, Djenadic et al. reported that the Li motion is localized in Li doped $MgAl_2O_4$ and therefore the long-range Li conductivity is insufficient for realization of an all-solid all-spinel battery [13].

Spinel is similar to garnet in that in both structures, the occupied tetrahedral and empty octahedral sites form an interconnected 3-D array for $Li^+$-ion transport. Conventional garnets are described by the formula $A_3B_3C_2O_{12}$ where A, B, and C have 8, 4, and 6 oxygen coordination, respectively. However, in garnet structured $Li_3Nd_3Te_2O_{12}$, where Li only occupies tetrahedral sites, the Li-ion is practically immobile at room temperature and ionic conductivity can only be measured at elevated temperature, only achieving $10^{-5}$ S cm$^{-1}$ at 600 °C [14]. In contrast, when additional Li is added to occupy both tetrahedral and octahedral sites in a "Li-stuffed" garnet such as $Li_5La_3Ta_2O_{12}$ [15] room temperature conductivity rises to $1.2 \times 10^{-6}$ S cm$^{-1}$. Further Li leads to even higher conductivity in $Li_{7-3x}La_3Zr_2Al_xO_{12}$ which has room temperature ionic conductivity greater than $10^{-4}$ S cm$^{-1}$ [1]. In this work, we studied a substitutional strategy to form a "Li-stuffed" spinel, with Li occupying both the tetrahedral 8a and octahedral 16d sites, in a somewhat analogous fashion to Li-stuffed cubic garnet. Since we have different energy (tetrahedral and octahedral) sites, the presence of Li on the octahedral sites tends to reduce the energy potential between the two sites making Li motion easier [16]. A room-temperature $Li^+$ ionic conductivity greater than $10^{-4}$ S cm$^{-1}$ is observed for the Li-stuffed spinel. In the composition of highest conductivity, $Li_{1.25}Cr_{0.25}Ti_{1.5}O_4$, the 8a tetrahedral site is fully occupied by Li and the 16d octahedral site is 75% occupied by Ti and the remaining 25% split evenly by Li and Cr. The remaining tetrahedral, 8b, and octahedral, 16c, are unoccupied. $Li_{1.25}Cr_{0.25}Ti_{1.5}O_4$ contains Ti(IV), which is unstable to Li reduction; however, the use of an interfacial layer such as $Li_3N$ or a conductive polymer can fix this problem [17] to enable its use with Li or $LiC_6$ anodes or more likely the concept can be used in solid solution formation with spinel-structured cathodes, where mixed electronic ionic conductivity is desirable. The integration of solid electrolytes with lithium has progressed rapidly since the report of high conductivity in garnet; however, there has been a lack of progress with cathode–solid electrolyte integration to achieve high ionic and electronic transport through the cathode [18,19]. Unlike conventional Li-ion cells where liquid electrolyte fills the cathode pores providing ion transport and carbon black provides electron transport, cathodes for all solid-state batteries require both ion-conducting as well as electron-conducting additives to enable mixed ionic/electronic transport. However, these solid–solid interfaces have high resistance compared to solid–liquid interfaces, and transport through composite cathodes is a major challenge to enable all solid-state batteries [20]. In a first small step towards application of the concept as solid-state catholyte, we show a solid solution of a Li-stuffed, spinel-structured electrolyte and the $LiNi_{0.5}Mn_{1.5}O_4$ high voltage, spinel-structured positive electrode material to be an electrochemically active cathode material in a liquid-containing cell thus showing that no high resistance solid–solid interfaces are formed.

## 2. Results

### *2.1. X-ray Diffraction (XRD) and Structural Refinement*

The XRD patterns of the $Li_{1.25}Cr_{0.25}Ti_{1.5}O_4$ (LCTO, bottom) and $Li_{1.25}AlTi_{1.5}O_4$ (LATO, top) powders are shown in Figure 1. The patterns are indexed to the cubic spinel structure, space group, $Fd\bar{3}m$. The LATO pattern has two small, unidentified peaks at 39.64 and 46.18° 2Θ which disappear after hot-pressing (Figure 2). The lattice parameters determined from Rietveld refinement and using Si as internal peak position standard are 8.3440 Å and 8.3574 Å for $Li_{1.25}Cr_{0.25}Ti_{1.5}O_4$ (LCTO) and, $Li_{1.25}AlTi_{1.5}O_4$ (LATO), respectively. Since, $Cr^{3+}$ is larger than $Al^{3+}$, 0.615 Å vs. 0.535 Å [21,22], the fact that the unit cell of LATO is larger than LCTO might suggest a small amount of $Al^{3+}$ mixing onto the tetrahedral 8a spinel site in exchange for $Li^+$ (0.76 Å) on the 16d octahedral site in the $Fd\bar{3}m$ space group. Site mixing is highly unlikely for $d^3$ $Cr^{3+}$ owing to its well-known high crystal field stabilization energy in octahedral coordination [23]. Site mixing of Al onto the 8a tetrahedral sites is common in spinels and is, for example, observed in $MgAl_2O_4$ [23]. Partial occupation of the 8a tetrahedral site by the heavier Al atom relative to Li would be evidenced in the XRD pattern by an increase in the intensity of the 220 (~30° 2Θ, Cu K α radiation) and the 422 (~54° 2Θ, Cu K α radiation) peaks [24].

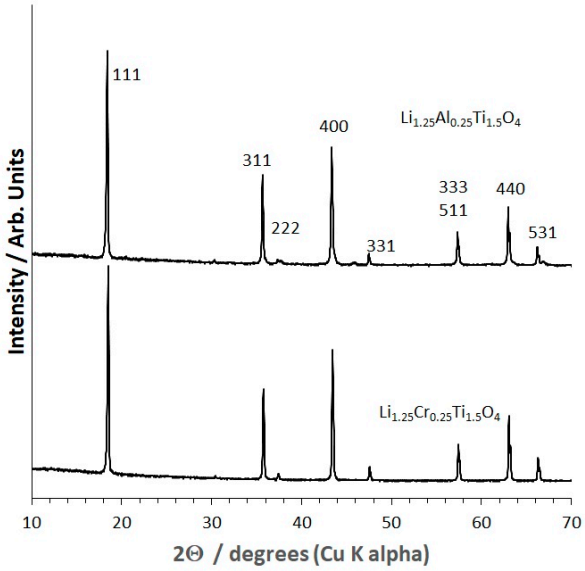


**Figure 1.** XRD of $Li_{1.25}Cr_{0.25}Ti_{1.5}O_4$ solid electrolyte powder (**bottom**) and $Li_{1.25}Al_{0.25}Ti_{1.5}O_4$ solid electrolyte powder (**top**). XRD peaks are indexed to the $Fd\bar{3}m$ spinel structure.

However, comparison of the LCTO XRD pattern versus the LATO XRD pattern (Figure 1) does not indicate any significant difference in the intensity of the peaks for the two samples, suggesting that any site mixing between Al and Li in LATO is negligible. The lack of significant site mixing is further evidenced from Rietveld structure refinement using power XRD data. Structural analysis by Rietveld refinement of XRD data was done with the Fullprof program [25].

The Rietveld refinement results are plotted with WINPLOTR program [26] in the supplementary information (Figures S1 and S2) and the atomic positions and final refinement information is contained in the supplementary information (Tables S1 and S2), for LCTO and LATO, respectively. In the starting Rietveld structural model for both LCTO and LATO, Li was placed on the 8a tetrahedral site, Li, Ti and Cr or Al were randomly distributed on the 16d octahedral site and oxygen on the 32e site of the $Fd\bar{3}m$ space group. During the refinement, site mixing of Ti, Al, or Cr on the 8a tetrahedral site was explored but led to a lower goodness of fit. That is, in the fully converged refinements, the 8a octahedral site is occupied by Li and the 16d octahedral site is randomly occupied by Li, Ti, and (Cr or Al). The oxygen positional parameter ($u$), the atomic position coordinate of oxygen in the 32e

site, was refined to a value of 0.26321 and 0.26340 for LCTO and LATO, respectively. The *u* values should be taken as an approximation since it is relatively difficult to locate oxygen positions through X-ray diffraction. Neutron diffraction will be needed to definitively define the oxygen position. The relative value of the positional parameter is in accordance with what is expected based on the relative sizes of $Cr^{3+}$ and $Al^{3+}$ [27]. If the origin of the unit cell is taken as the center of symmetry, in an ideal, cubic closed packed oxygen lattice, the oxygen parameter, *u*, has a value of 0.250. In the case of $u = 0.250$, the octahedral cation–oxygen bond length is 1.155 times longer than the tetrahedral–oxygen bond length [27]. However, the spinel oxygen parameter changes depend on the size and charge of the cations occupying the tetrahedral and octahedral sites, distorting the cubic closed packed oxygen lattice to accommodate different ions. In fact, more than 30 different ions of varying size can be accommodated in the spinel structure [27]. To accommodate large cations on the tetrahedral sites, oxygens are displaced along the [11] direction increasing the tetrahedral cation–oxygen bond length and concurrently decreasing the octahedral cation–oxygen bond length, leading to an increase in *u* and vice versa. Manipulation of the *u* parameter through changes in site occupation of octahedral sites might be a tool to optimize Li-ion conductivity in spinels.

In summary, both LCTO and LATO are single phase spinel structured materials with Li occupying 8a and 16d sites, Cr, Al and Ti randomly occupying the 16d sites in a nearly cubic close packed oxygen framework. The oxygen framework adjusts the positions of the oxygens within the unit cell to accommodate the relative difference in size of Cr versus Al.

XRD patterns of hot-pressed and $Li_3BO_3$ (LBO)-containing samples are shown in Figure 2, indicating no new peaks, i.e., no new phases, and retention of the single-phase spinel structure. LBO, a low-melting sintering aid, was added to increase density and thereby improve conductivity and mechanical properties.

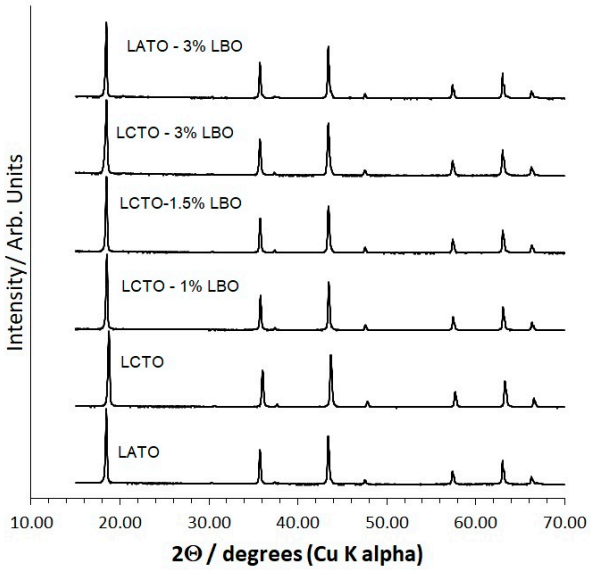


**Figure 2.** XRD of hot-pressed pellets of $Li_{1.25}Cr_{0.25}Ti_{1.5}O_4$ (LCTO) and $Li_{1.25}Al_{0.25}Ti_{1.5}O_4$ (LATO) with variable amounts of $Li_3BO_3$ (LBO). Pellets were ground to a powder prior to XRD data collection.

LBO is not detected in the XRD pattern owing to the light elements present and the low concentration. Generally, phases at or below a few weight% are not detected and some site substitution on spinel is also a possibility. The lattice constant as a function of $Li_3BO_3$ content for hot-pressed pellets was determined by grinding the pellets to a powder, the addition of NIST-traceable Si as an internal peak position standard and Rietveld refinement of the XRD pattern. The obtained lattice constants are tabulated and plotted in the supplementary information, Table S3 and Figure S3, respectively. In the case of LATO, there is an increase in the lattice constant of hot-pressed pellets with the addition

of 3% LBO to LATO from 8.3459(1) to 8.3474(1) Å. The LCTO lattice constants change in a more complicated manner. There is an initial increase in the lattice constant from 0% to 1% LBO, 8.3444(1) to 8.3456(1) Å and then a roughly linear decrease in lattice constant from 1, 1.5 and 3% LBO, 8.3456(1), 8.3450(1), 8.3449(1) Å, respectively. An increase might be attributed to substitution of additional relatively large Li onto the lattice and the decrease to substitution of the relatively small B. The evidence for site substitution by B is in agreement with the WDS analysis, which showed B distributed throughout the samples and not only at grain boundaries.

### *2.2. Microstructure*

Representative micrographs of the fracture surfaces of the hot-pressed LCTO sample without LBO (left) and with 1% LBO (right) are shown in Figure 3**.** From the SEM analysis, a couple of important points are noted. First, the LBO-containing sample is very dense in agreement with the high relative density ~98%, determined from the physical dimensions, weight and the theoretical density in contrast to the ~94% density of the sample without LBO. Almost no porosity is observable in the LBO-containing sample. A high relative density is extremely important for device applications because it leads to increased mechanical strength and higher ionic conductivity.

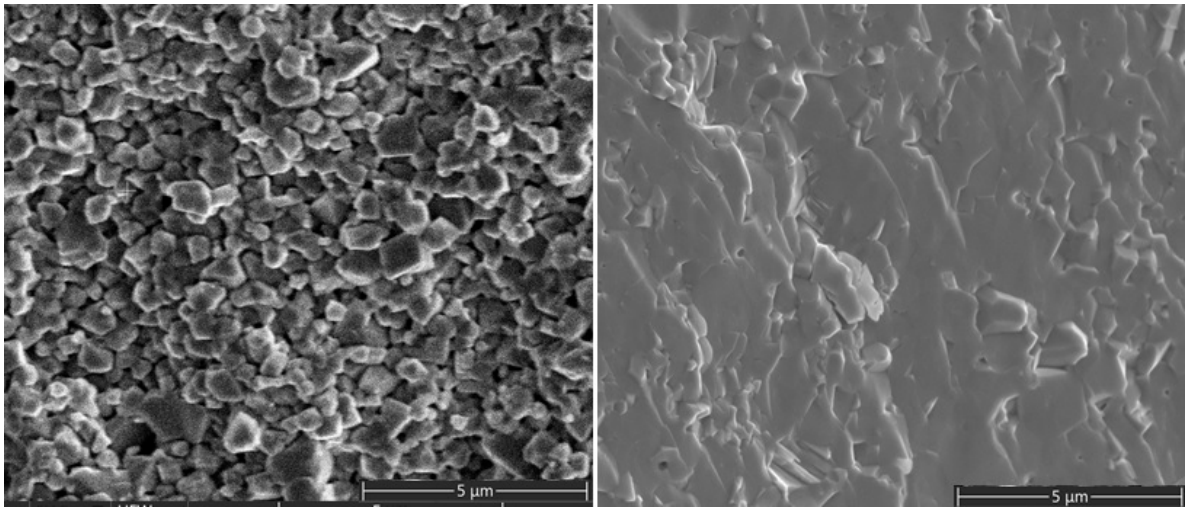


**Figure 3.** Representative SEM image of fracture surface images of hot-pressed $Li_{1.25}Cr_{0.25}Ti_{1.5}O_4$ without LBO, **left**, and with 1% LBO, **right**.

Second, the fracture surface is very flat indicating transgranular fracture revealing high grain boundary strength, which should lead to low inter-granular ionic resistance whereas for the LBO free sample the fracture node is primarily intergranular leading to higher grain boundary resistance. Third, the average grain size observable for the LBO free sample is about 1 µm. In the LBO-containing sample, the grain size is roughly estimated to be about 2–5 µm, though the grains are difficult to distinguish.

### *2.3. Conductivity*

The room temperature impedance plot for hot-pressed $Li_{1.25}Cr_{0.25}Ti_{1.5}O_4$ (~94% relative density) and the equivalent circuit (inset) which models the data are shown in Figure 4. In the equivalent circuit, R refers to resistance, and CPE to constant phase element. The impedance spectra shows a single semi-circle at higher frequency and starts to level off at lower frequency, which we interpret as the precursor to an upward sloping line. A fit of the data, based on this interpretation using the indicated equivalent circuit, is included in the supplementary information (Figure S4, Table S4). The equivalent circuit for this system where ionic conduction is predominant includes $R_b$, bulk or intra-grain impedance,

$R_{gb}$, the grain boundary or inter-grain impedance, $CPE_{gb}$, the grain boundary constant phase element and $CPE_{int}$, the sample electrode interface or dual layer constant phase element which is physically attributed to charge build-up at the electrode [28–30]. Since we used Li-ion blocking electrodes, the shape of the curve represents a material, which is predominantly a Li-ion conductor with low electronic conductivity [28–30]. From Figure 4, several important points are noted.

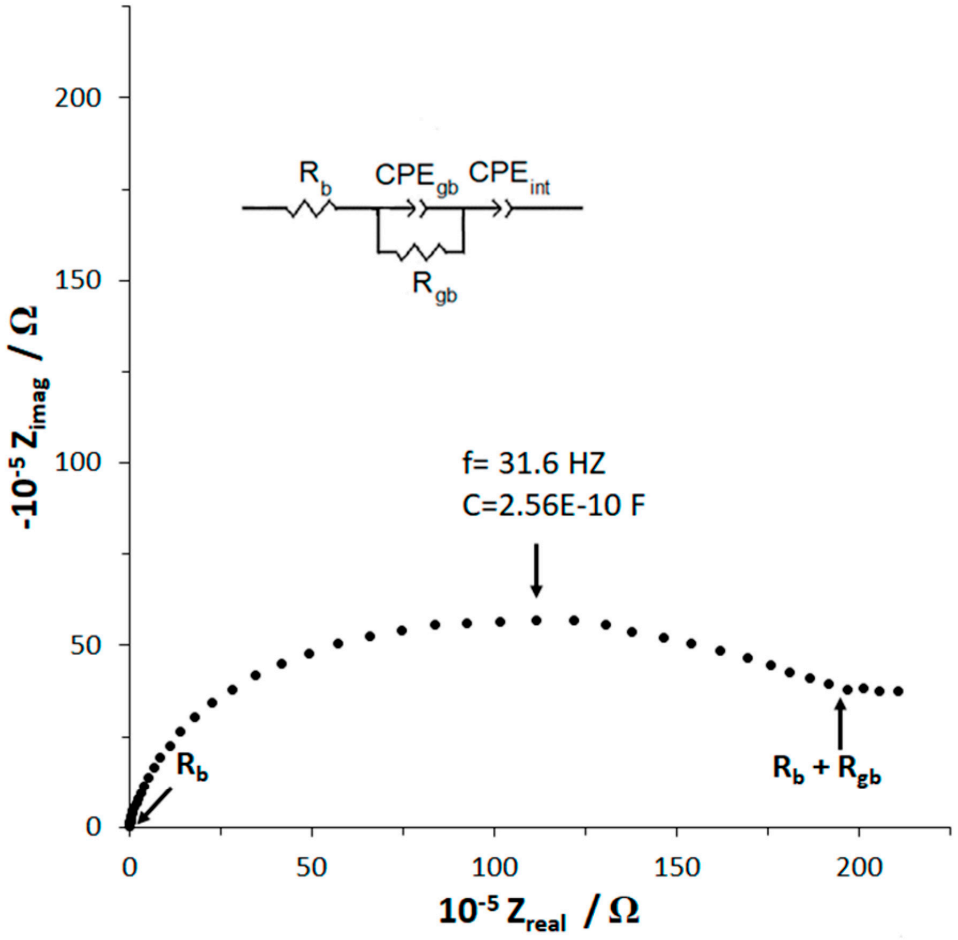


**Figure 4.** Room temperature impedance plot of hot-pressed $Li_{1.25}Cr_{0.25}Ti_{1.5}O_4$ and the equivalent circuit used to interpret the data.

First, the calculated value of the capacitance using the frequency at the maximum point of the semi-circle is shown on Figure 4. This capacitance, $2.56 \times 10^{-10}$F, was calculated from $C_{gb} = (2\pi f R)^{-1}$, using $f$ = 31 Hz and R (diameter of the semi-circle) = $1.97 \times 10^5$ Ω [31]. Second, this capacitance value is characteristic of a grain boundary [31] confirming the assignment of this semi-circle to a grain boundary phenomenon. The bulk impedance value, $R_b$ can be taken from the $Z_{real}$ intercept at the high frequency of the semi-circle and the total impedance, $R_{total} = R_b + R_{gb}$, is taken from the $Z_{real}$ low frequency intercept. Third, the values of $R_b$ and $R_{gb}$ and the physical dimensions of the sample are then used to determine the Li-ion conductivity. The bulk ionic conductivity of the $Li_{1.25}Cr_{0.25}Ti_{1.5}O_4$ pellet at room temperature is $1.63 \times 10^{-4}$ S cm$^{-1}$ and the total ionic conductivity of $Li_{1.25}Cr_{0.25}Ti_{1.5}O_4$ is $2.84 \times 10^{-8}$ S cm$^{-1}$. This bulk ionic conductivity is in the range of Al substituted $Li_7La_3Zr_2O_{12}$ cubic garnet solid-state electrolyte when first reported by Murugan et al. [1], however, the total ionic conductivity is three to four orders of magnitude lower than cubic garnet indicating relatively high grain boundary impedance. In fact, the ratio of grain boundary impedance to the total ionic impedance is 99.93%. We compare the ratio of

grain boundary impedance to the total ionic impedance since we cannot calculate a grain boundary conductivity as the volume of the grain boundaries is unknown.

The electronic conductivity of $Li_{1.25}Cr_{0.25}Ti_{1.5}O_4$ at room temperature obtained from the steady state current found through DC polarization [32,33] is about $1.84 \times 10^{-8}$ S cm$^{-1}$. Thus, the ionic transport number, $t_{ionic}$, for Li-ions in $Li_{1.25}Cr_{0.25}Ti_{1.5}O_4$ ($t_{ionic} = \sigma_{ionic}/\sigma_{total}$, where $\sigma_{total} = \sigma_{ionic} + \sigma_{electronic}$; $\sigma_{ionic}$ is the total ionic conductivity) is about 0.6, confirming that $Li_{1.25}Cr_{0.25}Ti_{1.5}O_4$ is an ionic conductor, yet having a significant electronic conductivity. Similarly, $Li_{1.25}Al_{0.25}Ti_{1.5}O_4$ was prepared, densified through hot-pressing and analyzed. The bulk ionic, total ionic and electronic conductivities obtained from the 97% relative density $Li_{1.25}Al_{0.25}Ti_{1.5}O_4$ pellet are $5.11 \times 10^{-5}$, $4.08 \times 10^{-7}$, and $9.79 \times 10^{-8}$ S cm$^{-1}$, respectively, a slightly lower bulk conductivity but a slightly higher bulk ionic and electronic conductivity than that of the 94% relative density LCTO pellet. The ionic transport number, $t_{ionic}$, for Li-ions in $Li_{1.25}Al_{0.25}Ti_{1.5}O_4$ is 0.81, evidencing a higher ionic component compared to LCTO as might be expected owing to the substitution of more easily reducible $Cr^{3+}$ compared to $Al^{3+}$. The lower bulk conductivity in LATO relative to LCTO most likely results from the difference in lattice constant, since the Li content is similar. Similarly to LCTO, almost all ionic impedance in the LATO pellet, 99.20%, originates at grain boundaries.

In order to overcome the high grain boundary impedance and to increase the density of the samples, $Li_3BO_3$ (LBO) was used as a sintering and hot-pressing aid. The room temperature impedance plot of $Li_{1.25}Cr_{0.25}Ti_{1.5}O_4$ hot-pressed with 3 wt% LBO to form a pellet of 98% relative density and the equivalent circuit (inset) which models the data are shown in Figure 5. This figure will be used to illustrate the interpretation of the EIS data for all of the LBO-containing samples. From Figure 5, several points can be made. First, the capacitance is calculated as previously described in the discussion of Figure 4 for the first two semi-circles from higher (right) to lower frequency and the values are noted on Figure 5. The calculated capacitances are characteristic of grain boundary and bulk phenomena for the higher frequency and lower frequency semicircles, respectively.

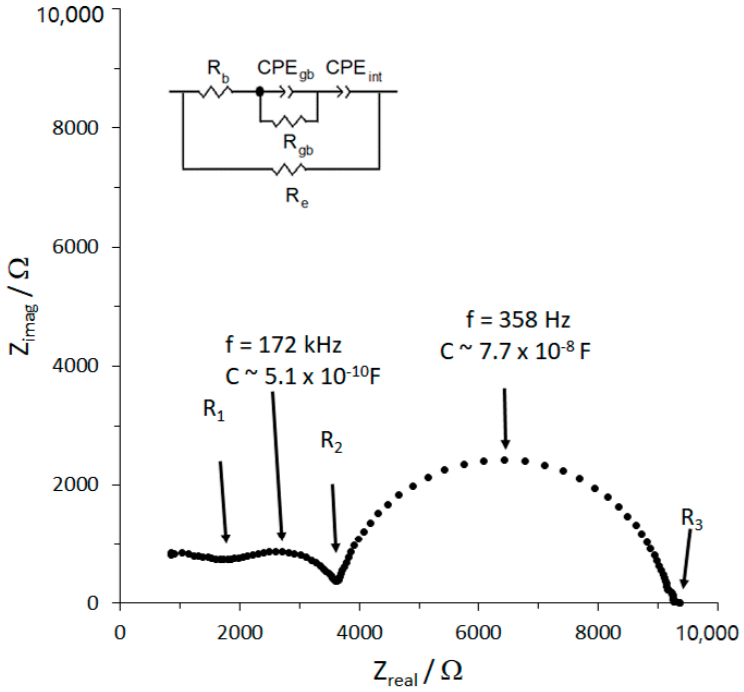


**Figure 5.** Room temperature impedance plot of hot-pressed $Li_{1.25}Cr_{0.25}Ti_{1.5}O_4$/3% LBO and the equivalent circuit used to interpret the data where $R_1 = R_eR_b/(R_e + R_b)$, $R_2 = R_e(R_b + R_{gb})/(R_e + R_b + R_{gb})$, and $R_3 = R_e$.

Second, the shape of the impedance plot is characteristic of an ionic conductor with electronic conductance [28], in agreement with the observation that hot-pressing with the LBO sintering aid changed the color of the samples from green (LCTO) and white (LATO) to black. Modelling the transport, therefore, requires the addition of a parallel electronic resistance, $R_e$, to the ionic-conduction circuit [28,29]. The values of the resistances in the equivalent circuit, bulk ionic resistance ($R_b$), grain boundary ionic resistance ($R_{gb}$), and electronic resistance ($R_e$) can be determined from the intercepts, $R_1$, $R_2$ and $R_3$, respectively, based on the following relationships: $R_1 = R_eR_b/(R_e + R_b)$, $R_2 = R_e(R_b + R_{gb})/(R_e + R_b + R_{gb})$, and $R_3 = R_e$ [28,29]. Finally, the values of $R_b$, $R_{ion}$, and $R_e$ and the physical dimensions of the sample are then used to determine the Li-ion and electronic conductivities.

For the LBO-containing samples, two pellets were analyzed for each composition. The highest total ionic conductivity was found for the $Li_{1.25}Cr_{0.25}Ti_{1.5}O_4$/1 wt. % LBO composition and is $4.17 \times 10^{-4}$ S cm$^{-1}$. The room temperature total $Li^+$ ion conductivity measured for a pellet of $Li_{1.25}Cr_{0.25}Ti_{1.5}O_4$—1 wt.% LBO is near the range of the highest ever reported for an oxide [34]. By comparison, substituted cubic garnet $Li_7La_3Zr_2O_{12}$ has reported total Li-ion conductivity ranging from $5 \times 10^{-4}$ to $1 \times 10^{-3}$ S cm$^{-1}$ [34]. The percent of ionic impedance from the grain boundary dropped to 19.31% in this sample. The DC electronic conductivity of $Li_{1.25}Cr_{0.25}Ti_{1.5}O_4$/1 wt.% LBO averaged $3.8 \times 10^{-4}$ S cm$^{-1}$ which means this composition may have applicability as an anolyte or catholyte where mixed electronic and ionic conductivity is important. The AC electronic conductivity value was in agreement with the DC measurement.

With the addition of 1 wt. % LBO, density increased, bulk ionic conductivity was slightly increased, total ionic conductivity increased by two to three orders of magnitude, and the electronic conductivity increased by four orders of magnitude. Thus, use of an optimal amount (~1 wt.%) of LBO might be particularly attractive to increase electronic conductivity and total ionic conductivity as a catholyte or anolyte. Data for all samples are tabulated in Table 1.

**Table 1.** Average room temperature (298 K) bulk ionic, $\sigma_{bulk}$, grain boundary ionic impedance as percentage of total impedance, $Z_{gb}/Z_{tot}$, total ionic conductivity, $\sigma_{ion}$, electronic conductivity, $\sigma_{elec}$ and relative density, D, of $Li_{1.25}CrTi_{1.5}O_4$ (LCTO) and $Li_{1.25}Al_{0.25}Ti_{1.5}O_4$ (LATO) solid electrolytes with and without $Li_3BO_3$ (LBO) sintering aid.

| Sample | $\sigma_{bulk}$ (S cm$^{-1}$) | $Z_{gb}/Z_{tot}$ (%) | $\sigma_{ion}$ (S cm$^{-1}$) | $\sigma_{elec}$ (S cm$^{-1}$) | D (%) |
|---|---|---|---|---|---|
| LCTO | $1.63 \times 10^{-4}$ | 99.9 | $1.19 \times 10^{-7}$ | $1.84 \times 10^{-8}$ | 94 |
| LATO | $5.11 \times 10^{-5}$ | 99.2 | $4.08 \times 10^{-7}$ | $9.79 \times 10^{-8}$ | 97 |
| LCTO/1% LBO | $6.77 \times 10^{-4}$ | 19.3 | $4.17 \times 10^{-4}$ | $3.76 \times 10^{-4}$ | 98 |
| LCTO/1.5% LBO | $4.01 \times 10^{-4}$ | 94.0 | $1.96 \times 10^{-4}$ | $1.78 \times 10^{-4}$ | 99 |
| LCTO/3% LBO | $8.75 \times 10^{-5}$ | 51.9 | $5.32 \times 10^{-5}$ | $4.06 \times 10^{-5}$ | 97 |
| LATO/3% LBO | $5.00 \times 10^{-5}$ | 27.4 | $1.78 \times 10^{-5}$ | $1.20 \times 10^{-7}$ | 99 |

Temperature-dependent conductivity data collection focused on the higher conductivity LBO-containing samples. Bulk ionic, grain boundary ionic, total ionic and electronic conductivities of $Li_{1.25}Cr_{0.25}Ti_{1.5}O_4$ (LCTO) and $Li_{1.25}Al_{0.25}Ti_{1.5}O_4$ (LATO) with varied weight percent LBO are shown in Figure 6 as a function of temperature. Log (1/Rgb) versus 1/T was plotted for the grain boundary data since one cannot calculate $\sigma_{gb}$ since the grain boundary volume is unknown and it only differs from plotting log($\sigma_{gb}$) versus 1/T by a constant [35]. In Figure 6, log σ is plotted as a function of 1/T in order to ease the reading of the conductivity values; however, all values of the activation energies $E_A$ were calculated based on log (σT) plotted as a function of 1/T, where σ is the conductivity (S cm$^{-1}$) and T is the temperature (K). For the 1/T vs. log (σT) plots, see the supplementary information, Figure S5. From Figure 6, several points can be made. First, all samples show fast room temperature Li-ion conductivity ranging from ~$10^{-4}$ to ~$10^{-3}$ S cm$^{-1}$ and comparable electronic conductivity, suggesting applicability as mixed ionic electronic conductors and the LCTO-1% LBO composition stands out for both high ionic and electronic conductivity. Use of these materials as solid electrolytes will require the discovery of an alternate sintering

aid or an alternate densification process to increase density and reduce grain boundary impedance perhaps under oxygen in order to maintain low electronic conductivity or the use of an interfacial layer such as $Li_3N$ [17]. However, it may find greater applicability as a catholyte or anolyte where mixed electronic ionic conductivity is desirable.

Turning attention to the bulk ionic conductivity activation energies, the values range from 0.18 to 0.28, 0.32 and 0.32, respectively for LCTO-1%LBO, LCTO-1.5%LBO, LCTO-3%LBO and LATO-3%LBO, respectively. The bulk activation energies are close to what is reported for other fast Li-ion conductors indicating fast Li-ion mobility [34,36–39].

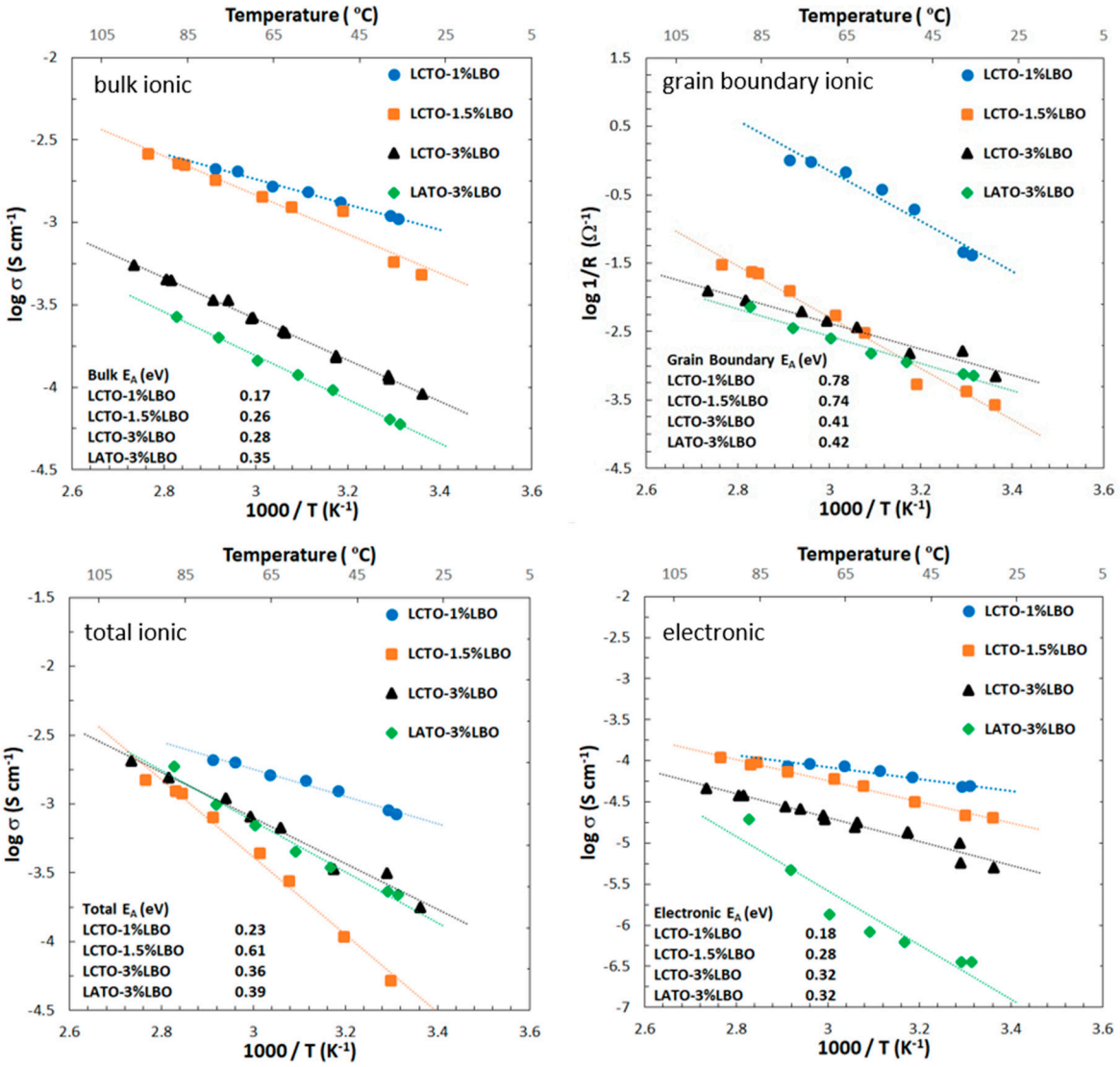


**Figure 6.** Bulk ionic, total ionic and electronic conductivities and ($1/R_{gb}$) grain boundary resistance plots of $Li_{1.25}CrTi_{1.5}O_4$ (LCTO) and $Li_{1.25}Al_{0.25}Ti_{1.5}O_4$ (LATO) with varied weight percent $Li_3BO_3$ (LBO) as a function of temperature. $E_A$ is the activation energy. Plotting ($1/R_{gb}$) was done since the grain boundary conductivity cannot be calculated because the grain boundary volume is unknown [35].

The especially low bulk activation energy of LCTO-1% helps to explain the very high Li-ion conductivity of this composition. These bulk activation energies are lower than the activation energy of 0.35 eV reported from Li NMR line broadening experiments on spinel-structured, Li-doped $MgAl_2O_4$ [12]. The grain boundary activation energies range from 0.78 to 0.74, 0.41 and 0.42 eV for LCTO-1%LBO, LCTO-1.5%LBO, LCTO-3%LBO and LATO-3%LBO, respectively, suggesting that the addition of a higher concentration of LBO has a strong effect to lower the activation energy for ionic conductivity at the grain boundary.

However, looking at the total ionic conductivities shows a clear superior performance for the LCTO-1%LBO sample, its total conductivity predominantly controlled by its higher bulk ionic mobility despite higher activation energy at its grain boundaries. The total ionic conductivity activation energies range from 0.23 to 0.61, 0.36, 0.39 eV for LCTO-1%LBO, LCTO-1.5%LBO, LCTO-3%LBO and LATO-3%LBO, respectively. The addition of excess LBO, >1%, negatively affects the total Li-ion conductivity although at 3% LBO the grain boundary ionic activation energy is considerably lower. The LCTO-1.5%LBO sample appears to be an outlier, as one would expect it to fall between the 1% and the 3% LBO samples. The electronic conductivities activation energies range from 0.18 to 0.28, 0.32, and 0.32 eV for LCTO-1%LBO, LCTO-1.5%LBO, LCTO-3%LBO and LATO-3%LBO, respectively. It is observed that at a low level of LBO the electronic conductivity is highest and as more LBO is added the electronic conductivity decreases. Overall, it appears that the 1%LBO sample has the maximum electronic and ionic conductivity. It might be that the higher electronic conductivity improves the ionic conductivity owing to an enhancement effect of the transport of two species [40–42]. That is, as a Li-ion hops, in order to preserve charge neutrality both species must move at the same speed which means the faster moving electron is slowed down while the speed of the slower moving $Li^+$ ion is increased.

### *2.4. Electrochemical Properties of Solid Solutions of $LiNi_{0.5}Mn_{1.5}O_4$ and "$Li_{1.25}Cr_{0.25}Mn_{1.5}O_4$"*

Demonstration of the practical applicability of $Li_{1.25}(Cr,Al)_{0.25}Ti_{1.5}O_4$ spinels as solid electrolyte to function as a separator will require finding a new densification aid that does not lead to high electronic conductivity. Subsequently, if such a densification aid is found, we will study the decomposition window of the electrolyte and build lithium symmetric cells. However, the use of the LBO densification aid leads to significant electronic conductivity, therefore this suggests that the most likely application of LBO-spinel composites is as catholyte or anolyte. Furthermore, the unique feature of demonstrating fast Li-ion conduction in spinel structured solids is the possibility to demonstrate that an electrochemically active solid solution can be formed from a solid solution with a spinel structured electrode material. A liquid based cell was used as a simple way to demonstrate this principle. Demonstration in a solid-state cell will require optimization of multiple properties and will be part of a future study.

Since $LiNi_{0.5}Mn_{1.5}O_4$ is known to form high-impedance phases when formed into a composite with $Li_7La_3Zr_2O_{12}$ garnet and other well-studied solid electrolytes, it was decided that it would be a good test case with practical applicability. We found that LCTO and LATO form single-phase, spinel-structured solid solutions with $LiNi_{0.5}Mn_{1.5}O_4$ and also $Li_4Ti_5O_{12}$. However, as a first test-case, Mn was substituted for Ti in the solid electrolyte component owing to the known deleterious effect of significant Ti substitution for Mn in $LiNi_{0.5}Mn_{1.5}O_4$ [43]. This substitution can be done to produce a Li-stuffed spinel of composition $Li_{1.075}Cr_{0.075}Ni_{0.35}Mn_{1.5}O_4$, though the $Li_{1.25}Cr_{0.25}Mn_{1.5}O_4$ end component could not be successfully synthesized owing to the formation of $Li_2MnO_3$ impurity. Follow-up studies will look in detail at the electrochemical properties, the mixed electronic-ionic conductivities, spinel phase stability, and electrochemical stability windows of the vast solid-solution range of materials in the families $Li_{1.25}(Cr,Al)_{0.25}(Mn,Ti)_{1.5})O_4$: $LiNi_{0.5}Mn_{1.5}O_4$ and $Li_{1.25}(Cr,Al)_{0.25}(Mn,Ti)_{1.5})O_4$: $Li_4Ti_5O_{12}$). The range of solid solution formation will be part of this future study. For the current study, we chose a 3:7 ratio to compare to a typical amount of porosity (30%) in a standard cell. In other words, the "electrolyte" component of the solid solution was set at 30%. This was a first estimate and is not yet optimized. The XRD pattern of nominal composition $0.3[Li_{1.25}Cr_{0.25}Mn_{1.5}O_4]$ $0.7[LiNi_{0.5}Mn_{1.5}O_4]$, i.e., $Li_{1.075}Cr_{0.075}Ni_{0.35}Mn_{1.5}O_4$ composition is shown in Figure 7. The lattice constant was refined to 8.1704(1) Å, which is comparable to $LiNi_{0.5}Mn_{1.5}O_4$ (8.1785 Å) [44] the predominant component of the solid solution. The slight decrease in the lattice constant is to be expected based on the slightly smaller average size of $Li^+$, $Cr^{3+}$ (0.76 Å, 0.615 Å, averaging 0.6875 Å) compared to $Ni^{2+}$ (0.69Å) in octahedral coordination [21,22]. The pattern is indexed to the cubic spinel structure, space group, $Fd\bar{3}m$, indicating a single-

phase composition of spinel structure. Structural analysis by Rietveld refinement of XRD data was done with the Fullprof program. The Rietveld refinement result is plotted in the supplementary information, Figure S6, and the atomic positions and final refinement information is contained in the supplementary information, Table S5. In the Rietveld structural model for $Li_{1.075}Cr_{0.075}Ni_{0.35}Mn_{1.5}O_4$, the 8a tetrahedral site is occupied by Li, the 16d octahedral site contains Li, Mn, Cr and Ni and oxygen occupies the 32e site of the $Fd\bar{3}m$ space group. During the refinement, site mixing of Cr, Ni or Mn on the 8a tetrahedral site was explored but did not improve the fit. That is, in the fully converged refinements, Li fully occupies the 8a tetrahedral and the 16d octahedral is randomly occupied by Li, Mn, Ni and Cr.

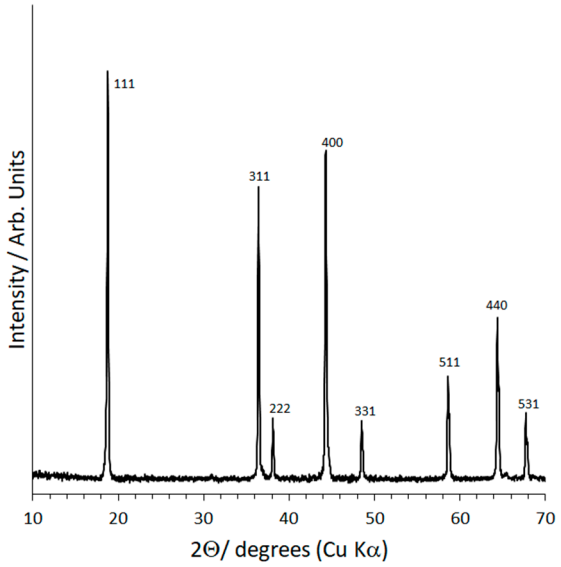


**Figure 7.** XRD pattern of 0.3 [$Li_{1.25}Cr_{0.25}Mn_{1.5}O_4$]: 0.7 [$LiNi_{0.5}Mn_{1.5}O_4$] solid solution formed at 850 °C (nominal composition: $Li_{1.025}Cr_{0.025}Ni_{0.45}Mn_{1.5}O_4$). XRD peaks are indexed to the $Fd\bar{3}m$ spinel structure.

The oxygen positional parameter ($u$), the atomic position coordinates of oxygen in the 32e site refined to a value of 0.26266, in accordance with expectation from the ionic radii of the tetrahedrally and octahedrally coordinated cations [27]. In order to demonstrate expediently that the $Li_{1.025}Cr_{0.025}Ni_{0.45}Mn_{1.5}O_4$ composition is electrochemically active, a liquid electrolyte-based cell was built. In the future, as composition, LBO content, microstructure and the ability to fabricate a thin, dense catholyte is optimized and developed, the concept will be tested in a solid-state configuration. The electrochemical discharge curve at 0.2C charge and discharge rate of the nominal composition 0.3[$Li_{1.25}Cr_{0.25}Mn_{1.5}O_4$] 0.7[$LiNi_{0.5}Mn_{1.5}O_4$], i.e., $Li_{1.075}Cr_{0.075}Ni_{0.35}Mn_{1.5}O_4$ composition is shown in Figure 8a. A discharge capacity ~120 mAh $g^{-1}$ is observed. Assuming electrochemical activity based on $Ni^{2+}/Ni^{3+}$, $Ni^{3+}/Ni^{4+}$ and $Cr^{3+}/Cr^{4+}$ couples yields a theoretical capacity of about 116 mAh $g^{-1}$ for $Li_{1.075}Cr_{0.075}Ni_{0.35}Mn_{1.5}O_4$. The theoretical discharge capacity is observed at >4.6 V. Additional capacity, beyond the theoretical, can be attributed to the $Mn^{3+}/Mn^{4+}$ couple observed as a shoulder around 4 V. The good rate performance resulting from high $Li^+$ ionic conductivity and electronic conductivity is shown in Figure 8b. The charge and discharge rates are varied from 0.2 to 10 C, with the charge and discharge rates remaining equal for each individual cycle. Additionally, the material shows good cycle life and no damage from the high rate of charge and discharge is evidenced as the capacity returns to 120 mAh $g^{-1}$ for 1 C after charging and discharging at 10 C rate. Further measurements and optimization of the mixed ionic electronic conductivity through composition and electrode design will be needed to fully realize the maximum rate performance. Further studies will be needed to characterize the conductivity of the solid electrolyte–solid cathode solid solu-

tions as a function of composition and with the addition of LBO to improve grain boundary conductivity. This preliminary result confirms the formation of an electrochemically active solid solution.

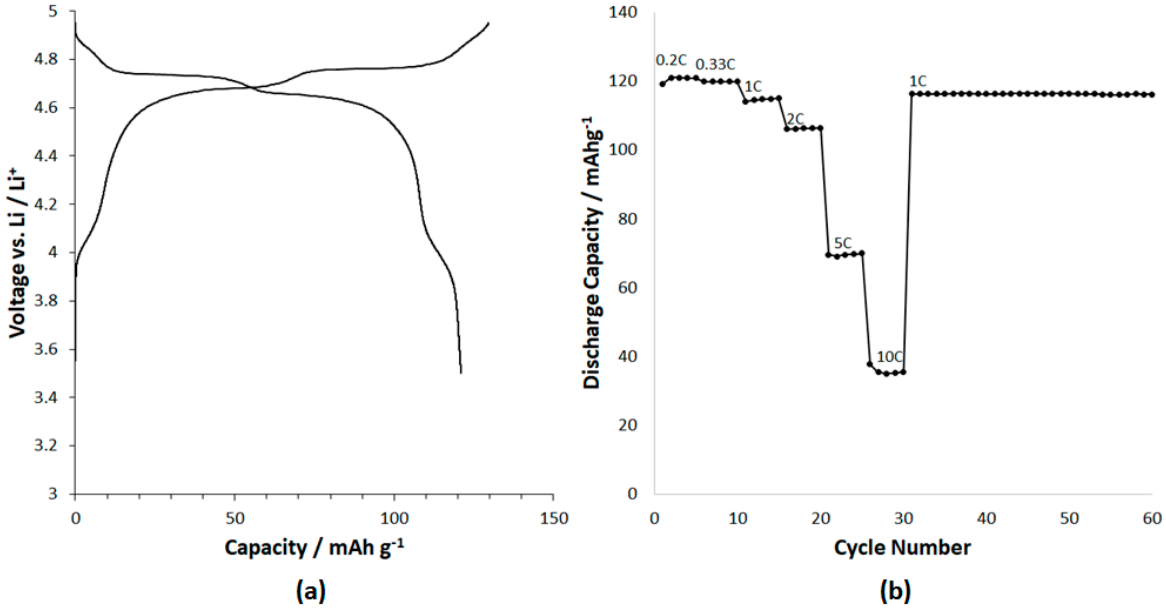


**Figure 8.** (**a**) Electrochemical charge and discharge curve of 30% $Li_{1.25}Cr_{0.25}Mn_{1.5}O_4$ and 70% $LiNi_{0.5}Mn_{1.5}O_4$ solid solution formed at 850 °C (nominal composition: $Li_{1.025}Cr_{0.025}Ni_{0.45}Mn_{1.5}O_4$) (**b**) Discharge capacity of $Li_{1.075}Cr_{0.075}Ni_{0.35}Mn_{1.5}O_4$ as function of charge and discharge rate at a loading of about 6 mg $cm^{-1}$ (~ 0.7 mAh $cm^{-1}$). Symmetrical charge and discharge rate indicated on the figure were varied each five cycles (cycles 1–30) and fixed at 1C for cycles 31–60.

### *2.5. Composition*

The elemental composition of the $Li_{1.25}Cr_{0.25}Ti_{1.5}O_4$ and $Li_{1.25}Al_{0.25}Ti_{1.5}O_4$ powders as obtained from ICP is tabulated in the supplementary information (Table S6) and is in excellent agreement with the nominal composition. In the LBO-containing samples, the semi-quantitative distribution of boron (B) was probed by wavelength dispersive spectroscopy (WDS) analysis of the cross-section of two representative pellets with 1 and 3% LBO. Over multiple spots spanning the length thickness of the pellet, B was spread through the whole sample, suggesting that the B is not concentrated at the grain boundaries. Since it was not possible to differentiate the grain boundary from the bulk during the data collection, we cannot definitively locate B since there is some chance that the measurement were done only on grain boundary or only bulk spots, the spot size is rather large (5 μ) and the error in measurement (±2% based on counting statistics) is on the order of the concentration (1–3% LBO). However, the analysis of XRD data and the changes in both bulk and grain boundary conductivity described later all support the conclusion that B is distributed throughout the sample. The B distribution from WDS is tabulated in the supplementary information (Table S7) and the images of the pellets used for determination of B distribution are shown in Figure S7.

## 3. Discussion

The introduction of Li on multiple sites has been previously demonstrated to be a successful strategy to attain higher $Li^+$ ion conductivity [1,15,16]. As an example, in garnet structured $Li_7La_3Zr_2O_{12}$, one of the most well-known oxide-based $Li^+$ conductors ($10^{-3}$ to $10^{-4}$ S $cm^{-1}$ at room temperature) $Li^+$ is sited on both tetrahedral (24d) and octahedral (96h) sites and the occupancy ratio between the sites is critical to optimization of the conductivity [45]. Similarly, the bulk ionic conductivity of $LiTi_2(PO_4)_3$ jumps by 3 orders of magnitude when additional Li occupies another crystallographic site as a result of partial

substitution of $Ti^{4+}$ by $Al^{3+}$ to form $Li_{1.3}Ti_{0.7}Al_{0.3}(PO_4)_3$ [46,47]. By contrast, $LiNi_{0.5}Ge_{1.5}O_4$ of modest $Li^+$ conductivity ($10^{-8}$ S $cm^{-1}$ at 63 °C) has Li only on the tetrahedral 8c site and Ni and Ge ordered 1:3 over the 4b and 12d octahedral sites of the ordered $P_432$ spinel.

The high Li-ion conductivity observed in LCTO and LATO can be compared to the $Fd\bar{3}m$ spinel structured anode $Li_4Ti_5O_{12}$ which has been reported to be a rather poor Li ion conductor [48–50] based on Li-NMR studies. This Li-NMR study is in conflict with the fact that $Li_4Ti_5O_{12}$ is a high-rate anode material [51,52], and that discrepancy was attributed by the authors to a fast ion conducting interphase which forms immediately upon Li insertion. Another study based on muon spin spectroscopy of $Li_4Ti_5O_{12}$ and $LiTi_2O_4$ spinels come to a different conclusion. Their muon spectroscopy results point to very mobile Li ions in $Li_4Ti_5O_{12}$ and lower activation energy for Li motion relative to $LiTi_2O_4$ [53]. In $Li_4Ti_5O_{12}$, the 8a tetrahedral site is occupied by Li as in LCTO and LATO, and the 16d octahedral site is occupied by Li and Ti in ratio of 1:5. In $LiTi_2O_4$, Li only occupies the 8a tetrahedral site and Ti completely occupies the 16d octahedral site. This is therefore further evidence of the positive effect of multiple site occupation on Li mobility.

Integration of solid electrolytes into electrodes has been problematic thus far in published studies of solid-state batteries. Density functional theory (DFT) computational studies have shown reactivity of cubic garnet structured $Li_7La_3Zr_2O_7$ and common Li-ion cathode materials [54,55] and experimental studies have shown the reactivity of $LiNi_{0.5}Mn_{1.5}O_4$ cathode with LLZO during electrochemical cycling [56]. Furthermore, $LiCoO_2$ forms unfavorable interfaces during densification and requires a $LiNbO_3$ coating to reduce reactivity [57]. Solid solutions of $Li_{1.25}(Al,Cr)_{0.25}(Ti,Mn)_{1.5}O_4$ with known electrode materials such as $LiNi_{0.5}Mn_{1.5}O_4$, e.g., $x[LiNi_{0.5}Mn_{1.5}O_4]$ $1\text{-}x[Li_{1.25}(Al,Cr)_{0.25}(Ti,Mn)_{1.5}O_4]$ ($0 < x < 1$) with grain boundary engineering through use of LBO or other sintering aids offer an alternative, simpler route since the solid electrolyte-solid electrode interface is eliminated and the LBO increases the electronic conductivity, which is needed for use as an electrode. This should lead to increased power owing to improved Li-ion and electronic conductivity within the electrode and the solid solutions could be used as part of an all solid-state battery with a garnet based separator and Li metal anode. If a new sintering aid is found that does not lead to electronic conductivity, these spinel electrolytes might be used in a fully spinel structured all-solid battery as envisioned by Thackeray and Goodenough [11] or with an interfacial layer such as $Li_3N$ [17] separating it from a Li metal or carbon anode. The $LiNi_{0.5}Mn_{1.5}O_4$ spinel is particularly attractive for solid-state application owing to its high energy storage density, high voltage (~4.7 V), use of abundant chemicals, small lattice change during charge and discharge and high Li diffusivity throughout the range of Li composition [58].

## 4. Materials and Methods

### *4.1. Powder Preparation*

The compound $Li_{1.25}Cr_{0.25}Ti_{1.5}O_4$ was prepared by solid-state reaction from a stoichiometric ratio of $TiO_2$ (Sigma-Aldrich, Saint Louis, MO, USA) and $Cr_2O_3$ (Alfa Aesar, Ward Hill, MA, USA) and a 3% stoichiometric excess of $Li_2CO_3$ (Alfa Aesar, Ward Hill, MA, USA) to counteract volatilization of Li. The precursors were ground by hand using a mortar and pestle, then the fine, mixed powder was heated in an uncovered alumina crucible at 10 °C per minute to 600 °C and held at this temperature for 10 h in air and allowed to furnace cool. The resulting powder was reground and pelletized using a SPEX Sample Prep 13 mm diameter pellet die (Spex Sampleprep LLC, Metuchen, NJ, USA) and Carver laboratory press (Fred S. Carver Company, Wabash, IN, USA) at a load of about 2300 kg. The pellet was placed in a covered alumina crucible and heated at 10 to 850 °C and held at this temperature for 24 h in air and then allowed to furnace cool. $Li_{1.25}Al_{0.25}Ti_{1.5}O_4$ and $Li_{1.25}Cr_{0.25}Mn_{1.5}O_4$ was prepared similarly substituting $Al_2O_3$ (Alfa Aesar, Ward Hill, MA, USA) for $Cr_2O_3$ and $MnCO_3$ for $Al_2O_3$ or $Cr_2O_3$, respectively. $Li_3BO_3$ (LBO) was prepared from a stoichiometric mixture of $Li_2CO_3$ (Alfa Aesar, Ward Hill, MA, USA) and $H_3BO_3$ (Alfa Aesar, Ward Hill, MA, USA). The starting mixture was ground in a mortar and pestle and heated at 600 °C in

air for 4 h. Solid solutions of the solid electrolyte and the LNMO cathode were prepared through an aqueous solution based route from a mixture $Li_2CO_3$ (Alfa Aesar, Ward Hill, MA, USA), $MnCO_3$ (Alfa Aesar, Ward Hill, MA, USA), $Ni(OH)_2$ (Alfa Aesar, Ward Hill, MA, USA), $Cr(NO_3)_3.9H_2O$ (Alfa Aesar, Ward Hill, MA, USA) precursors dissolved in a citric acid (Sigma-Aldrich, Saint Louis, MO, USA)/nitric acid (Sigma-Aldrich, Saint Louis, MO, USA) solution. As an example, $Li_{1.075}Cr_{0.075}Ni_{0.35}Mn_{1.5}O_4$ was prepared from 0.2659 g $Li_2CO_3$ (3% excess) 1.1208 g $MnCO_3$, 0.2109 g $Ni(OH)_2$, and 0.2401 g $Cr(NO_3)_3.9H_2O$, 1 g citric acid and 6 g concentrated $HNO_3$ diluted to 30 mL with $H_2O$. The clear green solution obtained from heating the mixture was evaporated to dryness and then heated under air in a Lindbergh furnace at 10 °C per minute to 450 °C, held for 3 h, heated at 10 °C per minute to 850 °C, held for 6 h, then furnace cooled (Lindbergh/MPH, Riverside, MI, USA).

### *4.2. Consolidation of Samples for Conductivity Measurements*

Sintering to obtain dense pellets was attempted in air at 850 °C. Sintering pure $Li_{1.25}Cr_{0.25}Ti_{1.5}O_4$ led to pellets of low density (~60–70% relative density) and the temperature could not be increased owing to the formation of a ramsdellite-structured phase at higher temperature. The addition of LBO led to much higher density pellets (~80–85%). LBO was chosen owing to the fact that its melting point of ~700 °C is below the 850 °C consolidation temperature, so that it can act as a liquid-phase sintering aid and also because LBO itself has moderate ionic conductivity which might enhance conduction at the grain boundaries unlike other typical sintering additives such as LiF which are poor Li-ion conductors and have melting point above the temperature at which the samples are converted from the spinel to the ramsdellite structure. A similar spinel to ramsdellite phase transformation upon heating has been previously documented for $LiTi_2O_4$ [59]. Dense discs (>90%) were prepared by rapid induction hot-pressing (custom built by University of Michigan, Ann Arbor, MI, USA) without (93–97%) and with LBO (near 100%). For the higher conducting $Li_{1.25}Cr_{0.25}Ti_{1.5}O_4$, three different amounts of LBO were tested (1, 1.5 and 3 wt. %) in an attempt to optimize conductivity. For the $Li_{1.25}Al_{0.25}Ti_{1.5}O_4$, a 3 wt. % LBO-containing hot-pressed sample was prepared based on sintering studies to increase density. The powders were densified at 850 °C at 40 MPa for 40 min under Ar using a rapid induction hot-pressing technique. The spinel powders were hot-pressed in a graphite die. During the hot-pressing, the die is contained in a stream of Ar, creating a reducing atmosphere. After, densification in the presence of LBO, the pellets changed to a black color. In the absence of LBO, no color change was observed. Attempts to oxidize reduced LBO-containing samples at 850 °C in air, in the presence of mother power to reduce Li loss by heating under air, were unsuccessful. The bulk density of the sample was determined from the weight and physical dimensions. The relative density values were estimated by dividing the measured density by the theoretical crystal density based on the spinel structure and the measured lattice constants. The presence of 1–3 wt.% lower density LBO (2.16 g $cm^{-3}$ versus 3.48 and 3.61 g $cm^{-3}$ for LATO and LCTO, respectively) was used to calculate a theoretical density based on the rule of mixtures and the relative density of each sample was then calculated. This can vary from actual by 1–2% based on whether LBO is incorporated into spinel or present as a distinct separate phase.

### *4.3. X-ray Diffraction*

X-ray diffraction (Cu Kα radiation, Rigaku Miniflex 600, D/teX Ultra silicon strip detector, Rigaku Americas Inc., The Woodlands, TX, USA) was used to characterize the phase purity of the powders and the material after hot-pressing. To determine phase purity and for Rietveld structural analysis [60], data were collected from 10–90° 2θ at 0.02° increments at 4° per minute. Lattice constants were calculated from Rietveld Refinement of an X-ray diffraction pattern collected for the sample mixed with a NIST traceable Si internal peak position standard. Data were collected from 10–90° 2θ at 0.02° increments at 4° per minute. Rietveld refinements of XRD data were carried out in the $Fd\bar{3}m$ space

group with Li in 8a sites and Li, Cr or Al and Ti or Mn randomly distributed in 16d sites, occupancies fixed to the starting composition.

### *4.4. Elemental Analysis*

Elemental analysis of the powders was performed at Galbraith Laboratories (Galbraith Laboratories, Inc., Knoxville, TN, USA) using Inductively Coupled Plasma-Optical Emission Spectroscopy (ICP-OES). Manually fractured, hot-pressed pellet cross-sections containing $Li_3BO_3$ were analyzed for boron concentrations via WDS using a JEOL JXA-8900 Electron Probe Microanalyzer (EPMA, Jeol USA, Inc., Peabody, MA, USA) in the Advanced Imaging and Microscopy Laboratory (AIMLab) at the University of Maryland. Analyses were conducted with a beam current of 50 nA and accelerating voltage of 15 kV. The beam diameter was 5 microns. Boron K-alpha x-rays were observed using an LDEB ($Mo/B_4C$ layered synthetic microstructure) analytical crystal. Raw counts were corrected using a ZAF (Z, atomic number, A, absorption, F, fluorescence) algorithm.

### *4.5. Microstructure*

Hot-pressed pellets were manually fractured for cross-sectional microstructural analysis. Cross-sectional analysis was conducted using Thermo Fisher Helios (Thermo Fisher Scientific, Waltham, MA, USA) and an FEI Quanta 200F scanning electron microscopes under a 5kV accelerating voltage (FEI Company, Hillsboro, OR, USA).

### *4.6. Conductivity*

The temperature-dependent ionic conductivity was determined from AC impedance measurements with a Bio-logic VMP300 (Bio-logic USA, Knoxville, TN, USA) (applied frequency range 0.1 Hz to 7 MHz) and/or a Solartron Modulab (Ametek Scientific Instruments, Oak Ridge, TN, USA) (0.1 Hz–300 kHz) with an amplitude of 10–100 mV. Ni was sputtered on the top and bottom of the hot-pressed discs to serve as Li—blocking electrode. The equivalent circuit was modelled and each data set was normalized to the geometric dimensions of the disc to determine the Li-ion conductivity. The Li-ion conduction activation energies were determined from the Arrhenius plot of the relationship of the ionic conductivities to temperature in the range of ~298K to 373K.

The electronic conductivity at room temperature was measured using DC polarization measurements at a voltage of 2 V (Solartron Modulab, Ametek Scientific Instruments, Oak Ridge, TN, USA). The steady-state current and applied voltage were used to determine the resistance, which was converted to the electronic conductivity using the specimen dimensions. Electronic conductivity was also estimated from the AC impedance data.

### *4.7. Electrochemical Measurements*

Solid solution electrodes of composition $Li_{1.25}Cr_{0.25}Mn_{1.5}O_4$:$LiNi_{0.5}Mn_{1.5}O_4$ of 3:7 mole ratio ($Li_{1.075}Cr_{0.075}Ni_{0.35}Mn_{1.5}O_4$) were mixed with carbon and PVDF in an NMP slurry to produce an 80:15:5 composite coating of the active: carbon black: PVDF on an Al foil current collector. The active loading was ~6 $mg/cm^3$. The C rate was based on a capacity of 147 mAh $g^{-1}$ for $LiNi_{0.5}Mn_{1.5}O_4$. Coin cells (Hohsen, Al clad, Pred Materials, New York, NY, USA) were fabricated using an electrolyte 1 M $LiPF_6$ dissolved in EC:EMC 1:1 (weight ratio, Sigma-Aldrich, Saint Louis, MO, USA) and 2% tris (trimethylsilyl) phosphate (TCI Americas, Portland, OR, USA) an electrolyte stabilizing additive for use at high voltage [61] and Li foil (Johnson Matthey, Alpharetta, GA, USA) as anode. The electrochemical data was collected on a Maccor 4000 Battery cycler (Maccor Inc., Tulsa, OK, USA) The charge and discharge rates were equal for each charge/discharge cycle and charge and discharge rates were varied each five cycles (cycles 1–30) in order from 0.2C, 0.33C, 1C, 2C, 5C to 10C and then fixed at 1C for cycles 31–60.

## 5. Conclusions

Herein, we report the synthesis and the fast Li-ion conductivity of the spinel structured $Li_{1.25}$(Al or Cr)$_{0.25}$(Ti or Mn)$_{1.5}O_4$ and a solid solution with the $LiNi_{0.5}Mn_{1.5}O_4$ high voltage positive electrode as examples of a large class of fast Li-ion conducting potential electrolytes and cathodes based on the spinel structure. Bulk and total ionic conductivities for 1% LBO LCTO of $6.8 \times 10^{-4}$ and $4.2 \times 10^{-4}$ S cm$^{-1}$, respectively, is comparable to that of the first reported bulk and total conductivities of garnet structured Al substituted $Li_7La_3Zr_2O_{12}$ [1], $4.9 \times 10^{-4}$ and $5.1 \times 10^{-4}$ S cm$^{-1}$, respectively. Li is located on both octahedral and tetrahedral sites to form a fast 3D $Li^+$ ion conduction pathway in $Li_{1.25}(Al,Cr)_{0.25}(Ti,Mn)_{1.5}O_4$, potentially enabling the all-solid all-spinel-structured battery concept with $Li_4Ti_5O_{12}$ spinel structured anode and $LiMn_2O_4$ or $LiNi_{0.5}Mn_{1.5}O_4$ spinel structured cathode. Significant electronic conductivity of Cr-containing samples points towards application as a catholyte or anolyte in a solid solution with known spinel structured electrode materials. Sintering with LBO leads to a highly dense mixed ionic, electronic conductor which may have application as a catholyte or a coating layer to form an artificial solid electrolyte interface to reduce reactivity with electrolytes. Electrochemical activity in liquid electrolyte-containing cells has been demonstrated for solid solutions of $Li_{1.25}Cr_{0.25}Mn_{1.5}O_4$ and $LiNi_{0.5}Mn_{1.5}O_4$ with discharge capacity of near or greater than the theoretical capacity of $LiNi_{0.5}Mn_{1.5}O_4$ demonstrating the concept of a spinel catholyte and a spinel cathode reacted to form a single-phase solid solution of spinel structure. This is a small step towards demonstrating their potential applications as catholyte or anolyte in a fully solid-state electrode.

**Supplementary Materials:** The following are available online; Figure S1: Rietveld fit of $Li_{1.25}Cr_{0.25}Ti_{1.5}O_4$; Figure S2: Rietveld fit of $Li_{1.25}Al_{0.25}Ti_{1.5}O_4$; Figure S3: Lattice constants of LCTO and LATO pellets as a function of LBO content; Figure S4: Fit of LCTO EIS data to equivalent circuit; Figure S5: Log ($\sigma$T) or Log(T/$R_{gb}$) plotted as a function of 1/T used for determination of bulk ionic, grain boundary ionic, total ionic and electronic activation energies of LCTO and (LATO) with varied weight percent of LBO as a function of temperature; Figure S6: Rietveld fit of $Li_{1.075}Cr_{0.075}Ni_{0.35}Mn_{1.5}O_4$; Figure S7: SEM image of pellets used for analysis of B distribution; Table S1: Refined structural model of LCTO; Table S2: Refined structural model of LATO; Table S3: Lattice constants of LCTO and LATO as a function of LBO content; Table S4: Equivalent circuit elements and value for fit of LCTO EIS data; Table S5: Refined structural model of $Li_{1.075}Cr_{0.075}Ni_{0.35}Mn_{1.5}O_4$; Table S6: Elemental analysis of LCTO and LATO; Table S7: Boron distribution in LCTO pellets.

**Author Contributions:** J.L.A. conceptualization, methodology, validation, formal analysis, investigation, data curation, writing—original draft preparation, writing—review and editing, visualization, supervision; B.A.C., investigation, data curation; R.C., methodology, investigation, validation, data curation; M.J.W., methodology, investigation, validation, data curation, writing—review and editing; D.T.T., investigation, methodology; L.M., investigation, methodology; P.M.P., investigation, methodology, resources; J.S., resources, methodology, writing—review and editing, supervision; J.W., conceptualization, methodology, validation, writing—review and editing. All authors have read and agreed to the published version of the manuscript.

**Funding:** J.L.A. and D.T.T. acknowledge the U.S. Army Combat Capabilities Development Command Army Research Laboratory (ARL) for funding. B.A.C. acknowledges funding from the ARL's Historically Black Colleges and Universities/Minority Institutions (HBCU/MI) program and the Army Educational Outreach College Qualified Leader program. L.M. acknowledges ARL for providing financial support under the Dr. Brad. E. Forch Distinguished Postdoctoral Fellowship administered by the National Research Council.

**Institutional Review Board Statement:** Not applicable.

**Informed Consent Statement:** Not applicable.

**Conflicts of Interest:** The authors declare no conflict of interest.

**Sample Availability:** Samples of the compounds are available from the authors through collaborative agreement.

## References


1. Murugan, R.; Thangadurai, V.; Weppner, W. Fast Lithium Ion Conduction in Garnet-type $Li_7La_3Zr_2O_{12}$. *Angew. Chem. Int. Ed.* **2007**, *46*, 7778–7781. [CrossRef] [PubMed]
2. Thackeray, M.M.; David, W.I.F.; Bruce, P.G.; Goodenough, J.B. Lithium Insertion into Manganese Spinels. *Mater. Res. Bull.* **1983**, *11*, 461–472. [CrossRef]
3. Ota, T.; Yamai, I. Thermal Expansion Behavior of $NaZr_2(PO_4)_3$Type Compounds. *J. Am. Ceram. Soc.* **1986**, *69*, 1–6. [CrossRef]
4. Yamai, I.; Ota, T. Grain Size-Microcracking Relation for $NaZr_2(PO_4)_3$ Family Ceramics. *J. Am. Ceram. Soc.* **1993**, *76*, 487–491. [CrossRef]
5. Smith, S.; Thompson, T.; Sakamoto, J.; Allen, J.L.; Baker, D.R.; Wolfenstine, J. Electrical, mechanical and chemical behavior of $Li_{1.2}Zr_{1.9}Sr_{0.1}(PO_4)_3$. *Solid-State Ion.* **2017**, *300*, 38–45. [CrossRef]
6. Case, E.D. The effect of microcracking upon the Poisson's ratio for brittle materials. *J. Mater. Sci. Lett.* **1984**, *19*, 3702–3712.
7. Kim, Y.; Case, E.D.; Gaynor, S. The effect of surface-limited microcracks on the effective Young's modulus of ceramics. *J. Mater. Sci.* **1993**, *28*, 1910–1918. [CrossRef]
8. Jackman, S.D.; Cutler, R.A. The effect of microcracking on ionic conductivity in LATP. *J. Power Sources* **2012**, *218*, 65–72. [CrossRef]
9. Hupfer, T.; Bucharsky, E.C.; Schell, K.G.; Senyshyn, A.; Monchak, M.; Hoffmann, M.J.; Ehrenberg, H. Evolution of microstructure and its relation to ionic conductivity in $Li_{1+x}Al_xTi_{2-x}(PO_4)_3$. *Solid-State Ion.* **2016**, *288*, 235–239. [CrossRef]
10. Kawai, H.; Tabuchi, M.; Nagata, M.; Tukamoto, H.; West, A.R. Crystal chemistry and physical properties of complex lithium spinels $Li_2MM'_3O_8$ (M = Mg, Co, Ni, Zn; M' = Ti, Ge). *J. Mater. Chem.* **1998**, *8*, 1273–1280. [CrossRef]
11. Thackeray, M.M.; Goodenough, J.B. Solid State Cell Wherein an Anode, Solid Electrolyte and Cathode Each Comprise a Cu-Bic-Close-Packed Framework Structure. U.S. Patent No. 4,507,371, 26 March 1985.
12. Rosciano, F.; Pescarmona, P.P.; Houthoofd, K.; Persoons, A.; Bottke, P.; Wilkening, M. Towards a Lattice-Matching Solid-State Battery: Synthesis of a New Class of Lithium-Ion Conductors with the Spinel Structure. *Phys. Chem. Chem. Phys.* **2013**, *15*, 6107–6112. [CrossRef] [PubMed]
13. Djenadic, R.; Botros, M.; Hahn, H. Is Li-Doped $MgAl_2O_4$ a Potential Solid Electrolyte for an All-Spinel Li-Ion Battery? *Solid State Ion.* **2016**, *287*, 71–76. [CrossRef]
14. O'Callaghan, M.P.; Lynham, D.R.; Cussen, E.J.; Chen, G.Z. Structure and Ionic-Transport Properties of Lithium-Containing Garnets $Li_3Ln_3Te_2O_{12}$(Ln = Y, Pr, Nd, Sm−Lu). *Chem. Mater.* **2006**, *18*, 4681–4689. [CrossRef]
15. Thangadurai, V.; Weppner, W. $Li_6ALa_2Ta_2O_{12}$ (A = Sr, Ba): Novel Garnet-like Oxides for Fast Lithium Ion Conduction. *Adv. Funct. Mater.* **2005**, *15*, 107–112. [CrossRef]
16. Goodenough, J.B. Fast Ionic Conduction in Solids. *Proc. R. Soc. A* **1984**, *393*, 215–234. [CrossRef]
17. Xie, H.; Li, Y.; Goodenough, J.B. NASICON-Type $Li_{1+2x}Zr_{2-x}Ca_x(PO_4)_3$ with High Ionic Conductivity at Room Temperature. *RSC Adv.* **2011**, *1*, 1728–1731. [CrossRef]
18. Kerman, K.; Luntz, A.; Viswanathan, V.; Chiang, Y.-M.; Chen, Z. Review—Practical Challenges Hindering the Development of Solid-state Li Ion Batteries. *J. Electrochem. Soc.* **2017**, *161*, A1731–A1744. [CrossRef]
19. Bielefeld, A.; Weber, D.A.; Janek, J. Microstructural Modeling of Composite Cathodes for All-Solid-State Batteries. *J. Phys. Chem. C Nanomater. Interfaces* **2019**, *121*, 1626–1634. [CrossRef]
20. Kotobuki, M.; Munakata, H.; Kanamura, K.; Sato, Y.; Yoshida, T. Compatibility of $Li_7La_3Zr_2O_{12}$ Solid Electrolyte to All-Solid-State Battery Using Li Metal Anode. *J. Electrochem. Soc.* **2010**, *151*, A1076–A1079. [CrossRef]
21. Shannon, R.D.; Prewitt, C.T. Effective Ionic Radii in Oxides and Fluorides. *Acta Crystallogr. B* **1969**, *21*, 925–946. [CrossRef]
22. Shannon, R.D. Revised Effective Ionic Radii and Systematic Studies of Interatomic Distances in Halides and Chalcogenides. *Acta Crystallogr. A* **1976**, *31*, 751–767. [CrossRef]
23. Burdett, J.K.; Price, G.D.; Price, S.L. Role of the Crystal-Field Theory in Determining the Structures of Spinels. *J. Am. Chem. Soc.* **1982**, *101*, 92–95. [CrossRef]
24. Le, M.-L.-P.; Strobel, P.; Colin, C.V.; Pagnier, T.; Alloin, F. Spinel-Type Solid Solutions Involving $Mn^{4+}$ and $Ti^{4+}$: Crystal Chemistry, Magnetic and Electrochemical Properties. *J. Phys. Chem. Solids* **2011**, *71*, 124–135. [CrossRef]
25. Rodríguez-Carvajal, J. Recent Advances in Magnetic Structure Determination by Neutron Powder Diffraction. *Phys. B Condens. Matter* **1993**, *192*, 55–69. [CrossRef]
26. Roisnel, T.; Rodríquez-Carvajal, J. WinPLOTR: A Windows Tool for Powder Diffraction Pattern Analysis. Available online: https://www.scientific.net/MSF.378-381.118 (accessed on 28 April 2021).
27. Hill, R.J.; Craig, J.R.; Gibbs, G.V. Systematics of the Spinel Structure Type. *Phys. Chem. Miner.* **1979**, *1*, 317–339.
28. Huggins, R.A. Simple Method to Determine Electronic and Ionic Components of the Conductivity in Mixed Conductors a Review. *Ionics (Kiel)* **2002**, *8*, 300–313. [CrossRef]
29. Thangadurai, V.; Huggins, R.A.; Weppner, W. Use of Simple Ac Technique to Determine the Ionic and Electronic Conductivities in Pure and Fe-Substituted SrSnO3 Perovskites. *J. Power Sources* **2002**, *108*, 64–69. [CrossRef]
30. Bauerle, J.E. Study of Solid Electrolyte Polarization by a Complex Admittance Method. *J. Phys. Chem. Solids* **1969**, *31*, 2657–2670. [CrossRef]
31. Irvine, J.T.S.; Sinclair, D.C.; West, A.R. Electroceramics: Characterization by Impedance Spectroscopy. *Adv. Mater.* **1990**, *1*, 132–138. [CrossRef]

32. Kennedy, J.H.; Kimura, N.; Stuber, S.M. Measurement of electronic conductivity in Fe-doped β-alumina. *J. Electrochem. Soc.* **1982**, *129*, 1968–1973. [CrossRef]
33. Hema, M.; Selvasekerapandian, S.; Hirankumar, G.; Sakunthala, A.; Arunkumar, D.; Nithya, H. Structural and Thermal Studies of PVA:NH4I. *J. Phys. Chem. Solids* **2009**, *71*, 1098–1103. [CrossRef]
34. Wu, Z.; Xie, Z.; Yoshida, A.; Wang, Z.; Hao, X.; Abudula, A.; Guan, G. Utmost Limits of Various Solid Electrolytes in All-Solid-State Lithium Batteries: A Critical Review. *Renew. Sustain. Energy Rev.* **2019**, *109*, 367–385. [CrossRef]
35. Bayard, M.A. Complex Impedance Analysis of the Ionic Conductivity of $Na_{1+x}Zr_2Si_xP_{3-x}O_{12}$ Ceramics. *J. Electroanal. Chem.* **1978**, *91*, 201–209. [CrossRef]
36. Allen, J.L.; Wolfenstine, J.; Rangasamy, E.; Sakamoto, J. Effect of Substitution (Ta, Al, Ga) on the Conductivity of $Li_7La_3Zr_2O_{12}$. *J. Power Sources* **2012**, *206*, 315–319. [CrossRef]
37. Knauth, P. Inorganic Solid Li Ion Conductors: An Overview. *Solid-State Ion.* **2009**, *18*, 911–916. [CrossRef]
38. Harada, Y.; Ishigaki, T.; Kawai, H.; Kuwano, J. Lithium ion conductivity of polycrystalline perovskite $La_{0.67-x}Li_{3x}TiO_3$ with ordered and disordered arrangements of the A-site ions. *Solid-State Ion.* **1998**, *108*, 407–413. [CrossRef]
39. Adachi, G.-Y.; Imanaka, N.; Aono, H. Fast Li⊕ Conducting Ceramic Electrolytes. *Adv. Mater.* **1996**, *1*, 127–135. [CrossRef]
40. Wagner, C. The theory of the warm-up process. *Z. Phys. Chem.* **1933**, *21*, 25–41.
41. Weppner, W.; Huggins, R.A. Determination of the Kinetic Parameters of Mixed-conducting Electrodes and Application to the System $Li_3Sb$. *J. Electrochem. Soc.* **1977**, *121*, 1569–1578. [CrossRef]
42. West, A.R. *Solid-State Chemistry and Its Applications*, 2nd ed.; John Wiley & Sons: West Sussex, UK, 2014; p. 421.
43. Alcántara, R.; Jaraba, M.; Lavela, P.; Tirado, J.L.; Biensan, P.; de Guibert, A.; Jordy, C.; Peres, J.P. Structural and Electrochemical Study of New $LiNi_{0.5}Ti_xMn_{1.5-X}O_4$ Spinel Oxides for 5-V Cathode Materials. *Chem. Mater.* **2003**, *11*, 2376–2382. [CrossRef]
44. Liu, D.; Lu, Y.; Goodenough, J.B. Rate Properties and Elevated-Temperature Performances of $LiNi_{0.5-x}Cr_{2x}Mn_{1.5-x}O_4$ ($0 \leq 2x \leq 0.8$) as 5 V Cathode Materials for Lithium-Ion Batteries. *J. Electrochem. Soc.* **2010**, *151*, A1269. [CrossRef]
45. Thompson, T.; Sharafi, A.; Johannes, M.D.; Huq, A.; Allen, J.L.; Wolfenstine, J.; Sakamoto, J. A Tale of Two Sites: On Defining the Carrier Concentration in Garnet-Based Ionic Conductors for Advanced Li Batteries. *Adv. Energy Mater.* **2015**, *1*, 1500096. [CrossRef]
46. Aono, H.; Sugimoto, E.; Sadaoka, Y.; Imanaka, N.; Adachi, G. Ionic Conductivity of Solid Electrolytes Based on Lithium Titanium Phosphate. *J. Electrochem. Soc.* **1990**, *131*, 1023–1027. [CrossRef]
47. Monchak, M.; Hupfer, T.; Senyshyn, A.; Boysen, H.; Chernyshov, D.; Hansen, T.; Schell, K.G.; Bucharsky, E.C.; Hoffmann, M.J.; Ehrenberg, H. Lithium Diffusion Pathway in $Li_{1.3}Al_{0.3}Ti_{1.7}(PO_4)_3$ (LATP) Superionic Conductor. *Inorg. Chem.* **2016**, *51*, 2941–2945. [CrossRef] [PubMed]
48. Wilkening, M.; Amade, R.; Iwaniak, W.; Heitjans, P. Ultraslow Li Diffusion in Spinel-Type Structured $Li_4Ti_5O_{12}$—a Comparison of Results from Solid-state NMR and Impedance Spectroscopy. *Phys. Chem. Chem. Phys.* **2007**, *1*, 1239–1246. [CrossRef] [PubMed]
49. Wagemaker, M.; van Eck, E.R.H.; Kentgens, A.P.M.; Mulder, F.M. Li-Ion Diffusion in the Equilibrium Nanomorphology of Spinel $Li_{4+x}Ti_5O_{12}$. *J. Phys. Chem. B* **2009**, *111*, 224–230. [CrossRef]
50. Ganapathy, S.; Vasileiadis, A.; Heringa, J.R.; Wagemaker, M. The Fine Line between a Two-Phase and Solid-Solution Phase Transformation and Highly Mobile Phase Interfaces in Spinel $Li_{4+x}Ti_5O_{12}$. *Adv. Energy Mater.* **2017**, *1*, 1601781. [CrossRef]
51. Wang, G.X.; Bradhurst, D.H.; Dou, S.X.; Liu, H.K. Spinel Li[Li1/3Ti5/3]O4 as an Anode Material for Lithium Ion Batteries. *J. Power Sources* **1999**, *83*, 156–161. [CrossRef]
52. Panero, S.; Reale, P.; Ronci, F.; Albertini, V.R.; Scrosati, B. Structural and Electrochemical Study on $Li(Li_{1/3}Ti_{5/3})O_4$ Anode Material for Lithium Ion Batteries. *Ionics (Kiel)* **2000**, *6*, 461–465. [CrossRef]
53. Sugiyama, J.; Nozaki, H.; Umegaki, I.; Mukai, K.; Miwa, K.; Shiraki, S.; Hitosugi, T.; Suter, A.; Prokscha, T.; Salman, Z.; et al. Li-Ion Diffusion In $Li_4Ti_5O_{12}$ and $LiTi_2O_4$ battery Materials Detected by Muon Spin Spectroscopy. *Phys. Rev. B Condens. Matter Mater. Phys.* **2015**, *91*. [CrossRef]
54. Miara, L.J.; Richards, W.D.; Wang, Y.E.; Ceder, G. First-Principles Studies on Cation Dopants and Electrolyte | cathode Interphases for Lithium Garnets. *Chem. Mater.* **2015**, *21*, 4040–4047. [CrossRef]
55. Zhu, Y.; He, X.; Mo, Y. First Principles Study on Electrochemical and Chemical Stability of Solid Electrolyte–Electrode Interfaces in All-Solid-State Li-Ion Batteries. *J. Mater. Chem. A Mater. Energy Sustain.* **2016**, *4*, 3253–3266. [CrossRef]
56. Hänsel, C.; Afyon, S.; Rupp, J.L.M. Investigating the All-Solid-State Batteries Based on Lithium Garnets and a High Potential Cathode—$LiMn_{1.5}Ni_{0.5}O_4$. *Nanoscale* **2016**, *1*, 18412–18420. [CrossRef]
57. Ohta, N.; Takada, K.; Sakaguchi, I.; Zhang, L.; Ma, R.; Fukuda, K.; Osada, M.; Sasaki, T. $LiNbO_3$-Coated $LiCoO_2$ as Cathode Material for All Solid-State Lithium Secondary Batteries. *Electrochem. Commun.* **2007**, *9*, 1486–1490. [CrossRef]
58. Xia, H.; Meng, Y.S.; Lu, L.; Ceder, G. Electrochemical Properties of Nonstoichiometric $LiNi_{0.5}Mn_{1.5}O_{4-\delta}$ Thin-Film Electrodes Prepared by Pulsed Laser Deposition. *J. Electrochem. Soc.* **2007**, *151*, A737. [CrossRef]
59. Gover, R.K.B.; Irvine, J.T.S.; Finch, A.A. Transformation of $LiTi_2O_4$ from Spinel to Ramsdellite on Heating. *J. Solid-State Chem.* **1997**, *131*, 382–388. [CrossRef]
60. Rietveld, H.M. A Profile Refinement Method for Nuclear and Magnetic Structures. *J. Appl. Crystallogr.* **1969**, *2*, 65–71. [CrossRef]
61. Allen, J.L.; Allen, J.L.; Thompson, T.; Delp, S.A.; Wolfenstine, J.; Jow, T.R. Cr and Si Substituted-$LiCo_{0.9}Fe_{0.1}PO_4$: Structure, Full and Half Li-Ion Cell Performance. *J. Power Sources* **2016**, *327*, 229–234. [CrossRef]